Southern Illinois University Carbondale
OpenSIUC

Publications

Department of Geography and Environmental Resources

4-6-2015

High resolution projections of 21st century daily precipitation for the contiguous USA

Justin T. Schoof
Southern Illinois University Carbondale, jschoof@siu.edu

Follow this and additional works at: http://opensiuc.lib.siu.edu/gers_pubs

Recommended Citation
Schoof, Justin T. "High resolution projections of 21st century daily precipitation for the contiguous USA." *Journal of Geophysical Research* (Apr 2015). doi:10.1002/2014jd022376.

This Article is brought to you for free and open access by the Department of Geography and Environmental Resources at OpenSIUC. It has been accepted for inclusion in Publications by an authorized administrator of OpenSIUC. For more information, please contact opensiuc@lib.siu.edu.

AGU PUBLICATIONS

JGR

Journal of Geophysical Research: Atmospheres

RESEARCH ARTICLE
10.1002/2014JD022376

Key Points:
- High-resolution precipitation projections are developed for the United States
- Increases are related primarily to precipitation intensity
- Decreases are related primarily to precipitation occurrence

Correspondence to:
J. T. Schoof,
jschoof@siu.edu

Citation:
Schoof, J. T. (2015), High-resolution projections of 21st century daily precipitation for the contiguous U.S., *J. Geophys. Res. Atmos.*, *120*, 3029–3042, doi:10.1002/2014JD022376.

Received 31 JUL 2014
Accepted 13 MAR 2015
Accepted article online 17 MAR 2015
Published online 16 APR 2015

High-resolution projections of 21st century daily precipitation for the contiguous U.S.

J. T. Schoof[1]

[1]Department of Geography and Environmental Resources, Southern Illinois University, Carbondale, Illinois, USA

Abstract Changes in precipitation have the potential to produce wide ranging impacts across human and natural systems. Here precipitation projections from select Atmosphere-Ocean General Circulation Models and Earth Systems Models participating in Phase 5 of the Coupled Model Intercomparison Project are downscaled to a high-resolution (0.25° × 0.25°) grid covering the contiguous U.S. to improve spatial and temporal characteristics of the model-derived projections and derive multiple descriptors of 21st century precipitation climate. Projections for the Northeast, Pacific Northwest, and the high elevations of the Rocky Mountains are characterized by increases in total annual precipitation, with the magnitude depending strongly on the level of radiative forcing. Parts of the southern U.S. are projected to experience moderate precipitation decreases under all forcing scenarios. Increases in total annual precipitation are associated primarily with changes in precipitation intensity during the cold season. Significant precipitation decreases are projected for parts of the southern U.S. in all seasons except autumn and are associated primarily with changes in precipitation occurrence. Many locations in the eastern U.S. are projected to experience longer extreme dry spells and longer extreme wet spells, reflecting an increase in the serial correlation of precipitation. Conversely, many western locations are projected to experience shorter dry spells and wet spells, reflecting a decrease in the serial correlation of precipitation. Most locations are projected to experience an increase in extreme precipitation, reflected in increases in the mean annual single-day maximum precipitation and the number of heavy (>10 mm) and very heavy (>20 mm) precipitation days.

1. Introduction

There is strong agreement among available data sets regarding a positive trend in annual precipitation over the Northern Hemisphere midlatitudes in recent decades [*Hartmann et al.,* 2013]. For most of the United States, the positive trend in total precipitation has been accompanied by increases in extreme precipitation [*Groisman et al.,* 2012*; Kunkel et al.,* 2013*; Villarini et al.,* 2013] with well-documented impacts on human and natural systems [*Easterling et al.,* 2000*; Parmesan et al.,* 2000*; Pryor et al.,* 2013]. However, parts of the west and southwest U.S. have experienced declining precipitation and model projections suggest further drying, with likely impacts on water resources [*Cayan et al.,* 2010]. Translating these changes to impacts on coupled natural human systems requires projections at higher resolution than that provided by contemporary climate models. This paper presents an approach that is well suited for projection of precipitation and its extremes.

Precipitation projections from Phase 5 of the Coupled Model Intercomparison Project (CMIP5) [*Taylor et al.,* 2012] Atmosphere-Ocean General Circulation Models (AOGCMs), and Earth Systems Models (ESMs) forced with high atmospheric greenhouse gases concentrations generally indicate changes in the United States that are smaller than one standard deviation of internal variability [*Collins et al.,* 2013], especially outside of winter. During the winter, CMIP5 models agree that precipitation will increase across the northern half of North America in association with elevated atmospheric moisture, increased moisture convergence, and a poleward shift in cyclone tracks. CMIP5 projections also indicate increases in extreme precipitation in both summer and winter [*Scoccimarro et al.,* 2013*; Toreti et al.,* 2013], resulting from both changes in circulation and increases in water vapor carried to regions of moisture convergence [*Meehl et al.,* 2005*; Tebaldi et al.,* 2006].

The coarse resolution of contemporary climate models limits their ability to provide output that can be directly used to assess impacts of climate change. Models often underestimate wet day precipitation intensity and overestimate precipitation occurrence [*Meehl et al.,* 2005*; Stephens et al.,* 2010*; Sillmann et al.,* 2013a], and because AOGCM-simulated precipitation represents an area average, extremes are frequently underestimated [e.g., *Harding et al.,* 2013]. Coarse model resolution also impacts the simulation of precipitation in regions of

©2015. American Geophysical Union. All Rights Reserved.

complex topography. As an example, *Mehran et al.* [2014] note that most CMIP5 models overestimate precipitation in the mountainous regions of western North America. Given the mismatch between coarse-resolution climate model output and high-resolution projections needed to assess climate change impacts across sectors, models are often downscaled dynamically using regional numerical models or statistically using methods ranging in complexity from simple scaling approaches to artificial neural networks and machine learning algorithms (see *Maraun et al.* [2010] and *Schoof* [2013] for recent reviews of statistical downscaling methods).

The various methodological approaches to precipitation downscaling have their relative merits and constitute a major source of uncertainty. To date, high-resolution precipitation projections for large geographic regions have been developed using only a small number of statistical approaches, with bias correction and spatial downscaling (BCSD) and constructed analogs (CAs) being the most common approaches for applications in the United States [see *Maurer and Hidalgo*, 2008; *Gutmann et al.*, 2014]. Application of BCSD at the daily time scale [as in *Thrasher et al.,* 2012] also results in binary precipitation occurrence values that do not vary at scales smaller than the climate model grid (i.e., it either rains or does not rain everywhere within a grid cell) [*Gutmann et al.,* 2014]. The CA approach may result in changes in statistics over monthly, seasonal, or annual time scales, but the daily values are limited to those in this historical record (or linear combinations thereof) [see *Hidalgo et al.,* 2008]. Additionally, the analogs are identified using data for the entire domain, which may impact the performance at small spatial scales [*Gutmann et al.,* 2014]. Methods based on pattern scaling have also become common (e.g., SimCLIM) [*Warrick et al.,* 2005] and promising new methods, such as asynchronous regional regression [*Stoner et al.,* 2013], are emerging.

In this study, a simple scaling method is combined with a stochastic weather model to generate high-resolution (0.25° × 0.25°) daily time series of precipitation for the contiguous United States, with the goal of improving both the spatial detail and the temporal characteristics of the model-derived precipitation projections at small scales. Since any number of small-scale weather sequences can be associated with a given large-scale condition, stochastic weather models are a natural and logical choice for use in downscaling [*Wilks,* 2010]. Here daily time series are generated for the period 2006–2095 for multiple climate models and three pathways for radiative forcing from greenhouse gases. The resulting time series are then analyzed to assess changes in total annual and seasonal precipitation as well as changes in the precipitation occurrence and intensity processes that lead to changes in precipitation extremes.

The high-resolution observed precipitation data and CMIP5 model data are described in section 2, along with the description of the downscaling method and stochastic weather model. The downscaling model is validated in section 3 and results from application to 21st century CMIP5 model projections are presented in section 4. The results are summarized and discussed in section 5.

2. Data and Methods

2.1. Data Sources

Daily precipitation data were taken from the Climate Prediction Center (CPC) 0.25° × 0.25° Daily U.S. Unified Precipitation data set [*Higgins et al.,* 2000]. In the construction of this data set, observations from between 8000 and 13,000 stations underwent extensive quality control and were then gridded using a modified *Cressman* [1959] scheme. The resulting grid consists of around 13,600 grid points covering the contiguous United States from 1948 to present. Here we used the data from 1948 to 2010. Hereafter, these are simply referred to as the observed precipitation data.

The AOGCMs and ESMs used in this study are a subset of CMIP5 models with daily precipitation output available for the historical period (1950–2005) and three 21st century radiative forcing pathways: BCC-CSM1.1 [*Xin et al.,* 2012], BNU-ESM, Can-ESM2 [*Arora et al.,* 2011; *von Salzen et al.,* 2013], CNRM-CM5 [*Voldoire et al.,* 2012], IPSL-CM5A-LR [*Dufresne et al.,* 2012], MPI-ESM-LR [*Stevens et al.,* 2013], MRI-CGCM3 [*Yukimoto et al.,* 2012], and NorESM1-M [*Bentsen et al.,* 2013]. As noted by *Knutti et al.* [2013], many contemporary AOGCMs share components, such their atmospheric models, so the effective number of models in the CMIP5 archive is considerably smaller than the actual number of models. The models used in this study represent a range of AOGCMs and ESMs and reflect the breadth of the hierarchy presented by *Knutti et al.* [2013]. The horizontal resolution of the models ranges from 1.125° × 1.125° (MRI-CGCM3) to 1.9° × 3.75° (IPSL-CM5A-LR).

©2015. American Geophysical Union. All Rights Reserved.

For each model, a single integration (usually the first member) was used. Additional details about the CMIP5 models can be found in *Taylor et al.* [2012]. The historical simulations used here are forced with historical greenhouse gas concentrations and time-evolving land cover. Model projections are based on the representative concentration pathways (RCPs) described by *Moss et al.* [2010]. Specifically, three RCPs are considered here, corresponding to low (RCP 2.6), medium (RCP 4.5), and high (RCP 8.5) levels of radiative forcing from greenhouse gases. To facilitate comparison between models and application of the downscaling technique, output from all of the models was interpolated to common 2.5° × 2.5° grid.

2.2. Stochastic Precipitation Model

Daily precipitation can be considered the result of two processes: occurrence and intensity. The former is a binary variable (precipitation either occurs or does not occur) whereas the latter describes how much precipitation occurs on wet days. The most common models for precipitation occurrence are based on Markov chains which were first applied by *Gabriel and Neumann* [1962]. *Schoof and Pryor* [2008] found that a precipitation occurrence model based on first-order Markov dependence sufficiently reproduced the observed distribution of wet and dry spell lengths for most U.S. locations, although more complex models performed better at locations in the western U.S. in agreement with the findings of *Wilks* [1999a]. Given a day where precipitation occurs, precipitation intensity must also be modeled. Common choices for wet day precipitation amounts include the two-parameter gamma distribution and the three-parameter mixed exponential distribution. While the latter was found to be superior for simulating monthly maxima by *Wilks* [1999a], the former performed nearly as well as it is much easier to represent in a downscaling algorithm, since the parameters can be easily derived from the mean and variance of wet day amounts.

In this study, the two-state (dry/wet), first-order Markov chain is used for precipitation occurrence. The model is defined by two transition probabilities, given by p_{01} (the probability of a wet day following a dry day) and p_{11} (the probability of a wet day following a wet day), which can be used to compute the climatological wet day probability (π) and the lag-1 autocorrelation of the precipitation occurrence process (r) [see *Wilks,* 1999b]. Precipitation amounts on wet days are randomly drawn from a gamma distribution with shape parameter α and scale parameter β. The mean (μ) and variance (σ^2) of the wet day precipitation amounts are then given by $\alpha\beta$ and $\alpha\beta^2$, respectively. The daily precipitation climatology for a location can therefore be conveniently summarized using the wet day probability (π), lag-1 autocorrelation of precipitation occurrence (r), and the mean (μ) and variance (σ^2) of wet day precipitation amounts, where the parameters are defined separately for each calendar month.

2.3. Downscaling Methodology

Application of the precipitation model described above in a downscaling context requires that a relationship is established between these four parameters at fine resolution and their coarse-resolution counterparts. Here the approach of *Wilks* [1999b] is adopted in which the high-resolution values are adjusted by the differences in the historical and future values. Rather than describe the method here, readers are directed to *Wilks* [1999b] for details. While the approach has been widely described in the literature, this is the first paper that has applied this approach to multiple climate models and radiative forcing pathways to produce projections of precipitation over a large region.

In this application, the CPC precipitation data are first aggregated from their native 0.25° × 0.25° resolution to a coarser 2.5° × 2.5° resolution, corresponding roughly to the resolution of contemporary climate models. The scaling between station precipitation statistics and their large-scale counterparts has been previously considered in the climate literature [see, for example, *Osborn and Hulme*, 1997]. In this application, the large-scale gridded precipitation is simply the average of the high-resolution gridded data, so extrapolation from unsampled regions is not a concern. The result of the aggregation is two sets of parameters corresponding to the historical coarse (hc)-resolution data (π_{hc}, r_{hc}, μ_{hc}, σ^2_{hc}) and historical fine (hf)-resolution (π_{hf}, r_{hf}, μ_{hf}, σ^2_{hf}) data. Development of downscaled future climate projections is then reduced to determining the future fine (ff)-resolution parameter set (π_{ff}, r_{ff}, μ_{ff}, σ^2_{ff}) corresponding to a future coarse (fc)-resolution parameter set, given by (π_{fc}, r_{fc}, μ_{fc}, σ^2_{fc}) and easily derived from the standard daily precipitation output provided by CMIP5 models.

The downscaled values of π and r are obtained by adjusting the historical fine-resolution values by the difference of the historical and future coarse-resolution values, following a log-odds transform that

©2015. American Geophysical Union. All Rights Reserved.

Table 1. Metrics Used to Characterize Current and Projected Precipitation Climates[a]

Abbreviation	Description
P_{wet}	Wet day probability
SDII	Simple daily intensity index: mean wet day precipitation intensity (mm)
P_{tot}	Precipitation total (mm)
RX1DAY	1 day maximum precipitation amount (mm)
R10mm	Number of heavy precipitation days (>10 mm)
R20mm	Number of very heavy precipitation days (>20 mm)
CDD	Maximum number of consecutive dry days
CWD	Maximum number of consecutive wet days

[a]As recommended by the World Meteorological Organization Commission for Climatology (CCI)/World Climate Research Programme (WCRP) project on Climate Variability and Predictability (CLIVAR) Expert Team on Climate Change Detection and Indices (ETCCDI).

maintains their natural bounds ($0 \le \pi \le 1$, $-1 \le r \le 1$). Downscaled values of the wet day precipitation mean and variance are assumed to be proportional to their coarse-resolution counterparts as described by *Wilks* [1999b]. The methodology therefore assumes that changes in π, r, μ, and σ^2 will be evenly distributed over the area with a grid cell of a climate model. To ensure that the large-scale changes represented by the parameter set (π_{fc}, r_{fc}, μ_{fc}, σ^2_{fc}) reflect changes in the model-simulated climate rather than differences between historical observations and historical climate model simulations, for the development of projections, both the historical and future parameter sets ((π_{hc}, r_{hc}, μ_{hc}, σ^2_{hc}) and (π_{fc}, r_{fc}, μ_{fc}, σ^2_{fc})) are defined using the climate model data.

The downscaled parameter set (π_{ff}, r_{ff}, μ_{ff}, σ^2_{ff}) can be conveniently used to generate daily precipitation time series as described by *Wilks* [1999b]. Given a generated series, a wider array of precipitation statistics can be considered. A subset of the indices developed by the World Meteorological Organization Commission for Climatology (CCI)/World Climate Research Programme (WCRP) project on Climate Variability and Predictability (CLIVAR) Expert Team on Climate Change Detection and Indices (ETCCDI) [see *Klein Tank et al.*, 2009] is used here to characterize contemporary and potential future precipitation climates (Table 1). These indices have been widely adopted in studies of historical climate variability and change [e.g., *Alexander et al.*, 2006; *Hartmann et al.*, 2013] and have recently been considered in the context of coarse-resolution CMIP5 simulations by *Sillmann et al.* [2013a, 2013b]. Wet day probability was not included in ETCCDI list of indices but is also considered here.

3. Model Validation

The applicability of the downscaling model described in section 2 to a changed climate was assessed by validating the model using analogs from the historical record as in *Wilks* [1999b]. Specifically, the CPC data were used to calculate the average U.S. precipitation for each year from 1948 to 2010. The 20 driest years and the 20 wettest years were then identified by ranking the mean annual total precipitation across all grid points. Using these criteria, the 20 driest years (in ranked order) are 1956, 1963, 1952, 1976, 1988, 1954, 2000, 1966, 1955, 2001, 1962, 1980, 1949, 2002, 1999, 1965, 1960, 1967, 1987, and 1989. The 20 wettest years (also in ranked order) are 1983, 1996, 1998, 1982, 1973, 1995, 1979, 1991, 1975, 1993, 1997, 1990, 2010, 2004, 1957 2009, 1992, 1986, 1972, and 2008. Using these data, parameter sets were computed using the CPC data at both fine- ($0.25° \times 0.25°$) and coarse- ($2.5° \times 2.5°$) resolution CPC data. The wettest 20 years were first considered as the baseline climate and the coarse-resolution parameter set from the driest 20 years was then considered as the future climate projection and used to derive corresponding fine-resolution statistics. The role of the wettest and driest years was then reversed so that the dry years provided the baseline and the wet years were the target. *Wilks* [1999b] used separation of wet and dry climates to validate the methodology. It is used here primarily to ensure that the method is capable of adapting to potentially large precipitation changes associated with changes in 21st century climate.

For each validation case, ten 20 year time series were generated. The resulting series were then used to compute a range of statistics (Table 1) and the mean of the 10-member ensemble was compared to the observed data for the validation period. Figure 1 shows the results for the wet day probability (P_{wet}), the simple daily intensity index (SDII; i.e., the mean wet day precipitation amount), and the total annual precipitation (P_{tot}) and indicates that the downscaling model coupled with the stochastic weather generator is able to reproduce the fine-scale variations in precipitation characteristics between wet and dry periods. The observed and generated differences between the wet years and dry years are shown in Figure 2. As expected, the difference between wet years and dry years in the downscaled data is largely manifest

©2015. American Geophysical Union. All Rights Reserved.

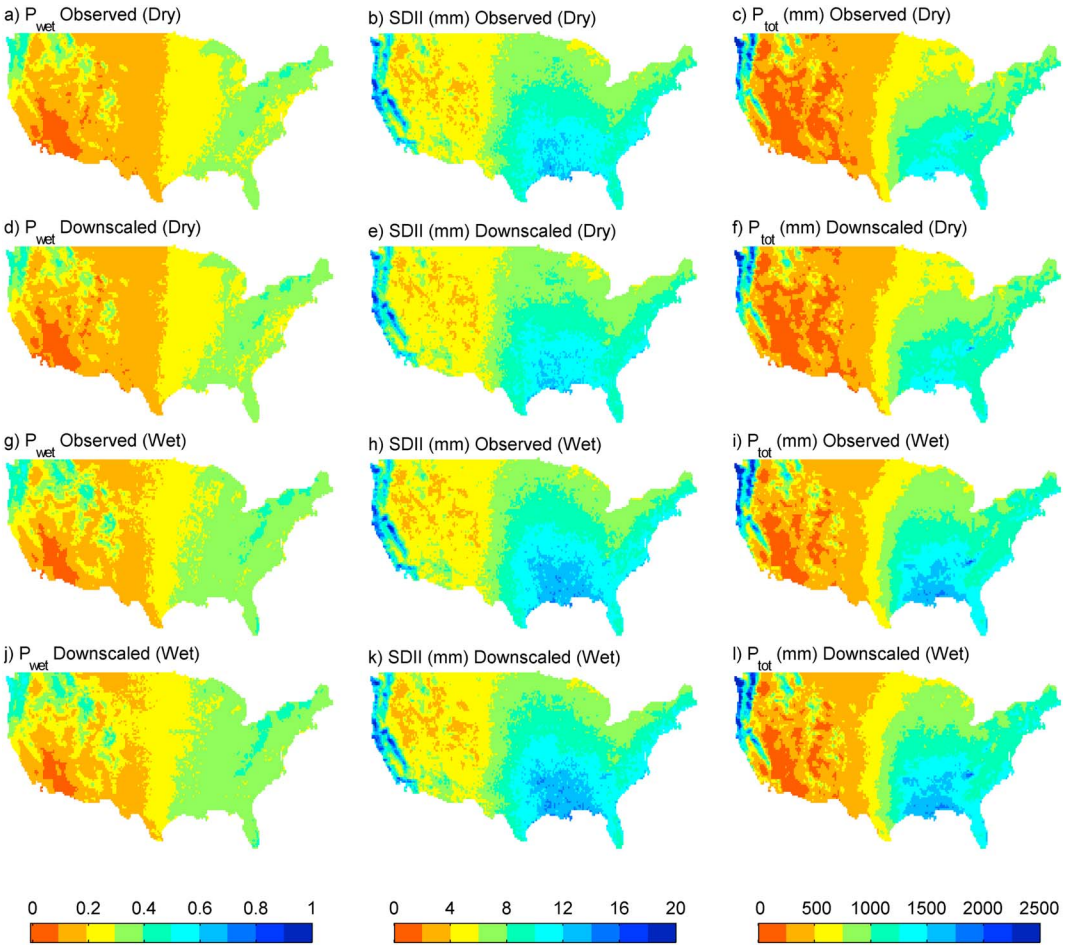

Figure 1. Observed and downscaled precipitation climates (a–f) for the driest 20 years and (g–l) for the wettest 20 years in the historical record as defined in section 3. Results are shown for the overall wet day probability (P_{wet}), the simple daily intensity index (SDII), and the total annual precipitation (P_{tot}).

as a coarse-resolution difference, but with some subgrid-scale variability that could not be derived from the coarse-resolution data alone. Averaged over the study region and the calendar year, the downscaled data exhibit a small positive bias in total precipitation during the wet validation period and a small negative bias during the dry validation period. These biases are smaller than those reported by *Gutmann et al.* [2014] for a range of downscaling methods applied to reanalysis data, although the comparison is only indirect since the downscaling conducted by *Gutmann et al.* [2014] focused on downscaling from reanalysis, the current validation exercise focuses on rescaling observed precipitation.

Validation statistics for the ETCCDI precipitation metrics indicate good agreement between the downscaled and observed data for the broad range of descriptors considered (Table 2). In addition to standard model evaluation statistics such as root-mean-square error (RMSE) and mean absolute error (MAE), Table 2 also shows two varieties of relative mean absolute error defined relative to observed value (RMAE1) and relative to the observed interannual variability (RMAE2). Errors tend to be slightly larger in both absolute value and relative to interannual variability for the wet years, but are similar relative to the magnitude of observed values. For both validation cases, statistics show better performance for ETCCDI metrics that depend only on daily values (e.g., P_{wet} and P_{tot}) and less well for wet and dry spells (e.g., CDD and CWD). Nevertheless, for all of the ETCCDI metrics considered, the average errors are small relative to both the magnitude of observed values and the observed interannual variability.

The validation experiment also provided an opportunity to examine the validity of the scaling assumption underlying the downscaling technique described in section 2.3. Because the future precipitation climate may differ substantively from the historical precipitation climate, a lack of consistency in the ratio of coarse-resolution

©2015. American Geophysical Union. All Rights Reserved.

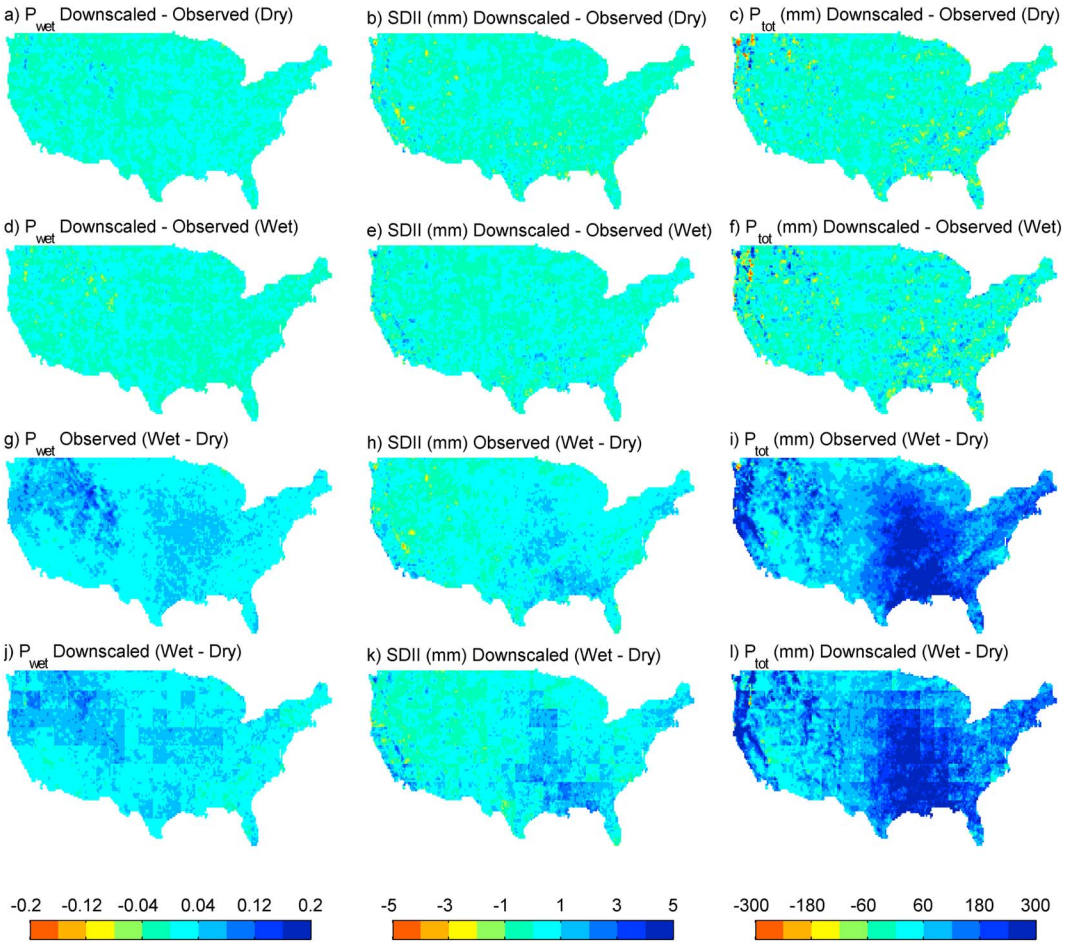

Figure 2. Differences between downscaled and observed (a, d) wet day probability (P_{wet}), (b, e) simple daily intensity index (SDII (mm)), and (c, f) total annual precipitation (P_{tot}) for the validation exercise. Also shown are the downscaled and observed differences between the wettest and driest 20 years in the historical record as defined in section 3. Results are shown for the overall (g, j) wet day probability (P_{wet}), (h, k) simple daily intensity index (SDII), and (i, l) total annual precipitation (P_{tot}).

to fine-resolution parameters during wet and dry periods could reduce confidence in projections. While the validation experiment described in this section addresses this to some extent, the difference in the ratios of coarse-resolution to fine-resolution values was additionally computed for each season and for each downscaled parameter (π, r, μ, and σ^2). The differences were generally small but were deemed statistically significant (on the basis of a Wilcoxon rank sum test with $\alpha = 0.05$) at some grid points for each test. The spatial distribution of points with significant differences did not exhibit any coherent spatial pattern. The proportion of points with significant differences was generally small, ranging from 0.05 to 0.11 depending on the season and parameter, reflecting a lack of evidence against the scaling assumption at most grid points.

4. Precipitation Projections

To develop future projections, the climate models described in section 2.1 were downscaled using the approach described in section 2.3. Rather than use the climate model grid point data directly, we average the output over nine grid points centered on the grid point of interest. For summary purposes, results are shown as differences between the multimodel ensemble median and historical observations (1950–2005) for three 30 year time periods representing the early, middle, and late 21st century: 2006–2035, 2036–2065, and 2066–2095. For each set of results, statistical significance was assessed by conducting a signed ranks test with $\alpha = 0.05$.

©2015. American Geophysical Union. All Rights Reserved.

Table 2. Validation Statistics for Statistical Downscaling[a]

	Dry Years				Wet Years			
	RMSE	MAE	RMAE1	RMAE2	RMSE	MAE	RMAE	RMAE2
				Annual				
P_{wet}	0.01	0.01	0.04	0.23	0.01	0.01	0.04	0.25
SDII	0.4	0.3	0.05	0.27	0.4	0.3	0.04	0.27
P_{tot}	40.9	27.4	0.05	0.20	48.5	33.2	0.05	0.22
RX1DAY	5.3	3.9	0.09	0.25	5.7	4.1	0.09	0.25
R10mm	2.0	1.5	0.10	0.30	2.6	2.0	0.11	0.37
R20mm	1.0	0.7	0.17	0.24	1.3	0.9	0.17	0.29
CDD	5.8	3.6	0.08	0.25	5.5	3.6	0.09	0.28
CWD	0.9	0.7	0.11	0.37	0.8	0.6	0.09	0.32
				DJF				
P_{wet}	0.02	0.01	0.07	0.37	0.02	0.01	0.07	0.35
SDII	0.7	0.5	0.08	0.39	0.6	0.5	0.07	0.38
P_{tot}	20.7	12.2	0.10	0.09	21.0	12.4	0.09	0.08
RX1DAY	3.7	2.6	0.12	0.17	4.3	2.9	0.12	0.18
R10mm	0.7	0.4	0.25	0.08	0.9	0.6	0.25	0.10
R20mm	0.4	0.3	0.37	0.09	0.5	0.3	0.38	0.09
CDD	2.9	2.1	0.09	0.17	2.8	2.0	0.10	0.19
CWD	0.6	0.5	0.12	0.23	0.7	0.5	0.12	0.24
				JJA				
P_{wet}	0.02	0.01	0.07	0.39	0.02	0.02	0.07	0.41
SDII	0.7	0.5	0.08	0.43	0.8	0.5	0.08	0.46
P_{tot}	16.0	11.7	0.08	0.09	18.2	13.4	0.08	0.10
RX1DAY	4.4	3.2	0.12	0.21	4.7	3.5	0.12	0.21
R10mm	0.8	0.6	0.17	0.12	0.9	0.7	0.17	0.14
R20mm	0.5	0.3	0.28	0.12	0.6	0.4	0.30	0.13
CDD	3.1	1.9	0.10	0.15	2.8	1.8	0.10	0.17
CWD	0.6	0.5	0.12	0.27	0.6	0.5	0.10	0.22

[a]The left-hand side of the table shows statistics resulting from developing the model using the 20 wettest years and then applying it to the 20 driest years. The right-hand side of the table shows statistics resulting from developing the model using the 20 driest years and then applying it to the 20 wettest years. Results are shown for the annual statistics as well as the winter (DJF) and summer (JJA) seasons. The metrics for describing the precipitation climate are described in Table 1. Statistics presented include root-mean-square error (RMSE), mean absolute error (MAE), and two formulations of relative mean absolute error defined as MAE divided by the mean value (RMAE1) and as the MAE divided by the standard deviation of annual or seasonal values (RMAE2).

Projected changes in annual total precipitation are presented in Figure 3. General features of the projections include a decline in precipitation in the Southwest U.S. and an increase in precipitation in the Northeast, in the high elevations of the Rocky Mountains, and in the Pacific Northwest. Given the similarity in radiative forcing in the early period, the relatively small differences in the maps are expected. The smallest changes are associated with the RCP 2.6 scenario, which is characterized by maximum CO_2 concentrations in the midcentury period and the lowest overall radiative forcing at the end of the century. For the RCP 4.5 and RCP 8.5 scenarios, the patterns of change are similar, but the intensity changes as a function of time and radiative forcing consistent with pattern scaling [*Tebaldi and Arblaster,* 2014]. As an example, note that the changes associated with moderate increases in radiative forcing during the late-century period (RCP 4.5, 2066–2095) closely resemble the changes associated with high levels of radiative forcing during the midcentury period (RCP 8.5, 2036–2065). Under high levels of radiative forcing, the late-century period is characterized by precipitation increases exceeding 200 mm per year in the high elevations of the Rocky Mountains and within the high-precipitation regions of the Pacific Northwest. Increases in precipitation are also projected for the Northeast region. Decreases of 50–100 mm per year are common for locations in southern Texas with small decreases for parts of the Southwest region. These results are qualitatively similar to those presented in summary graphics from larger ensembles of CMIP5 models [e.g., *Collins et al.,* 2013]. However, as shown in Figure 3, the higher spatial resolution associated with the downscaling application results in much greater spatial detail, especially in areas of substantive relief such as the intermountain West.

©2015. American Geophysical Union. All Rights Reserved.

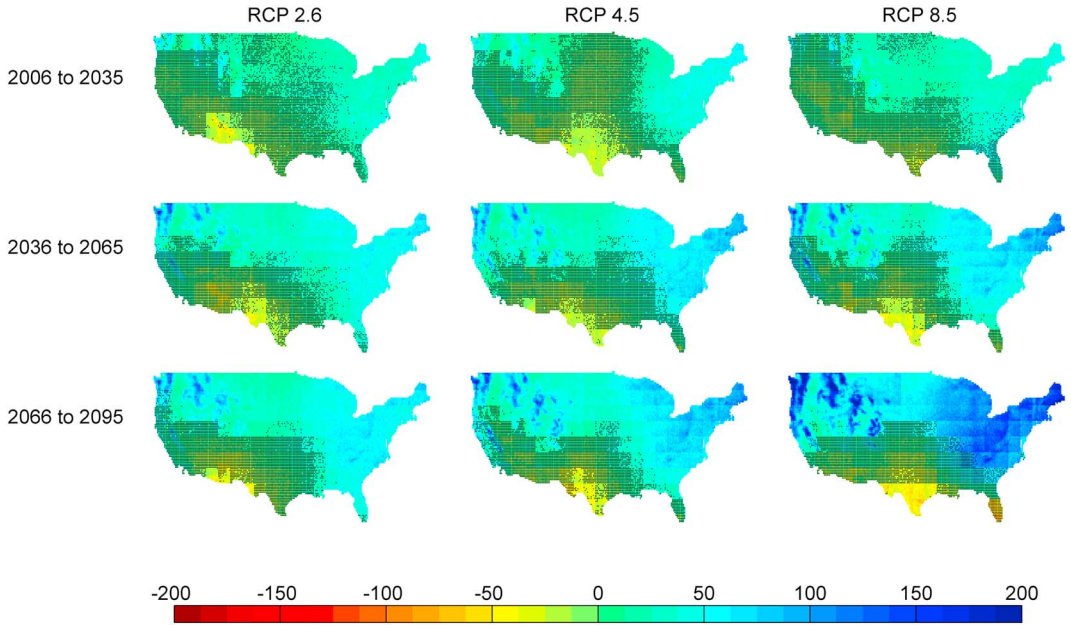

Figure 3. Projected changes in annual total precipitation (in mm) based on the ensemble mean of downscaled output from eight AOGCMs. Results are shown for the (top row) early 21st century, (middle row) middle 21st century, and (bottom row) late 21st century and for (left column) low, (middle column) medium, and (right column) high levels of radiative forcing from greenhouse gases. Changes in hatched areas are not significant at the 95% level.

Changes in annual total precipitation have the potential to mask important seasonal changes in precipitation. Furthermore, it is often important to differentiate between changes in total precipitation resulting from the occurrence and intensity processes described in section 2.2. Figure 4 shows the changes for each climatological season and for the wet day probability (P_{wet}), simple daily intensity index (SDII; mm), and the total seasonal precipitation (P_{tot}; mm). The projections differ substantively among the seasons, with the winter (December-January-February; DJF) and spring (March-April-May; MAM) projections for total precipitation bearing the strongest resemblance to the annual totals presented in Figure 3. During the summer (June-July-August; JJA), projected changes are not statistically significant for most regions, but small decreases in precipitation are projected for the south central U.S. and peninsular Florida. Across the Northern U.S., the changes in autumn (September-October-November; SON) precipitation are positive but are generally small relative to changes during winter and spring. The Southeast U.S. is projected to receive more precipitation during the autumn in contrast to the declines or insignificant changes projected for the other seasons. As with the annual totals, these seasonal changes are in good agreement with the coarse-resolution changes described for the CMIP5 multimodel ensemble by *Collins et al.* [2013], but with additional spatial detail in mountainous areas.

A notable feature of the projections is that, with the exception of a small number of grid points in the SW, all of the significant changes in precipitation intensity (SDII) are associated with increases (Figure 4). Regional decreases in total precipitation therefore tend to be associated with changes in the precipitation occurrence process. As shown in Figure 4, parts of the south and southwest U.S. are projected to experience as much as 10% fewer precipitation events during the late 21st century under strong radiative forcing in agreement with the findings reported by *Polade et al.* [2014]. Decreases in the frequency of wet days also explain the projected decline in summer precipitation in the south central U.S. as well as the differences in West Coast and Northeast U.S. projections during autumn relative to winter and spring.

Changes in precipitation frequency are also manifest as changes in the duration of dry spells and wet spells. Among the ETCCDI metrics (Table 1) are CDD, the mean annual maximum number of consecutive dry days, and CWD, the mean annual maximum number of consecutive wet days. Projections of CDD and CWD for the late-century period (2066–2095) are shown in Figure 5. A large increase in CDD is projected for some grid points in the Southwest, especially under high levels of radiative forcing. Increases of up to 4 days are projected for parts of the Eastern U.S. under all levels of radiative forcing. These findings are consistent with those of *Sillmann et al.* [2013b] who found an increase in dry spell length across the

©2015. American Geophysical Union. All Rights Reserved.

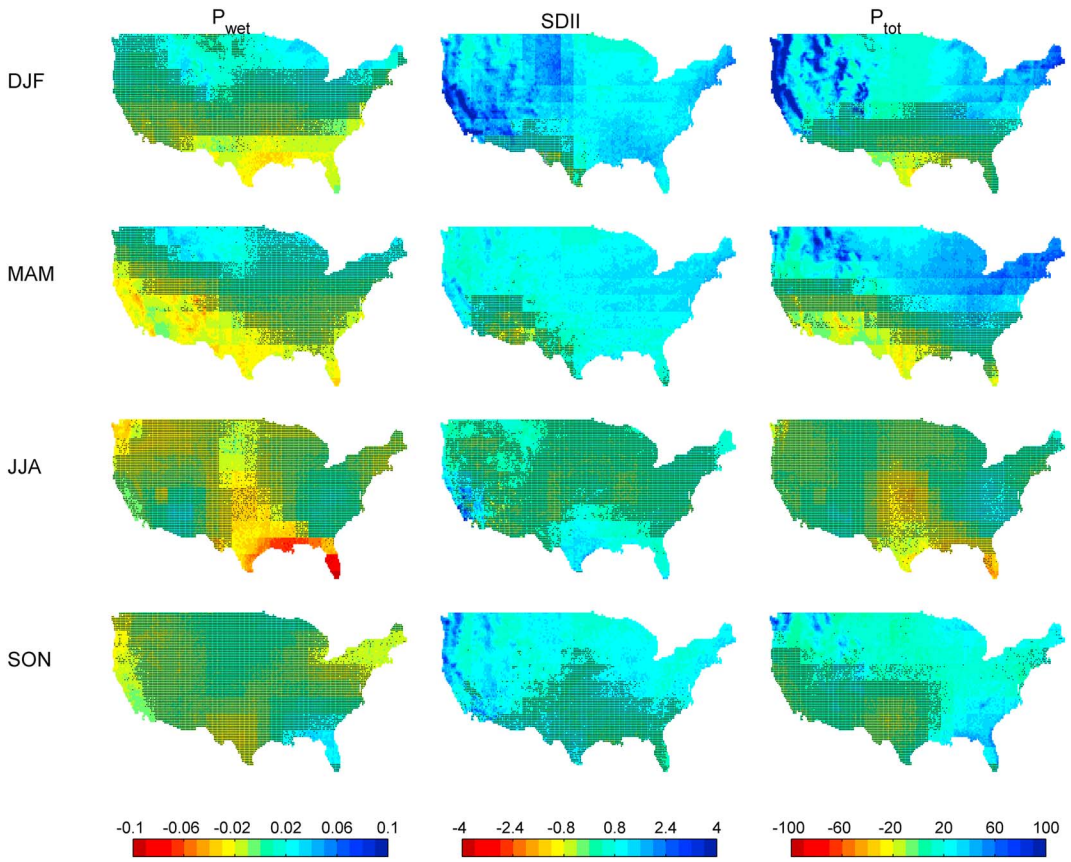

Figure 4. Projected changes in seasonal (left column) wet day probability (P_{wet}), (middle column) simple daily intensity index (SDII; mm), and (right column) total precipitation (P_{tot}; mm) under high radiative forcing (RCP 8.5) for 2066–2095. Results are based on the ensemble mean of downscaled output from eight AOGCMs. Changes in hatched areas are not significant at the 95% level.

Southern U.S. in a multimodel ensemble under the RCP 8.5 scenario. Under low levels of radiative forcing, the Northwest and Central U.S. are projected to experience shorter dry spell duration, with smaller decreases as radiative forcing increases (Figure 5). The mean annual maximum wet spell duration (CWD) is expected to increase in the Northeast U.S. and decrease along the Gulf Coast and Florida peninsula and throughout the Pacific Northwest. Combined with the projections of changes in daily precipitation intensity (Figure 4), these results suggest changes in the serial correlation of precipitation in several regions. In the northeast, the projections are characterized by more intense events separated by longer dry periods, while locations in the northwest are projected to experience larger events separated by shorter dry periods.

Projected increases in daily precipitation intensity drive an overall increase in the mean annual maximum single-day precipitation total (RX1DAY) as well as the number of heavy (>10 mm; R10mm) and very heavy (>20 mm; R20mm) precipitation days (Figure 6). With the exception of parts of the south, significant increases in RX1DAY are projected for most of the contiguous U.S. during winter and spring. Like the daily intensity (SDII) and total precipitation (P_{tot}), changes in RX1DAY are smallest during the summer and increases in RX1DAY are limited primarily to locations in the Northwest U.S. and extreme Northeast U.S. Extreme peninsular Florida is projected to experience a decrease in RX1DAY during summer. Projections for autumn are characterized by significant increases in RX1DAY for most locations in the western half of the U.S. as well as the Great Lakes region.

The number of heavy precipitation events tends to correlate with seasonal total precipitation, as noted by *Frich et al*. [2002]. As shown in Figure 6, the largest increases in R10mm and R20mm occur in regions of large seasonal precipitation change, such as the West Coast during winter, the Northeast U.S. during winter and

©2015. American Geophysical Union. All Rights Reserved.

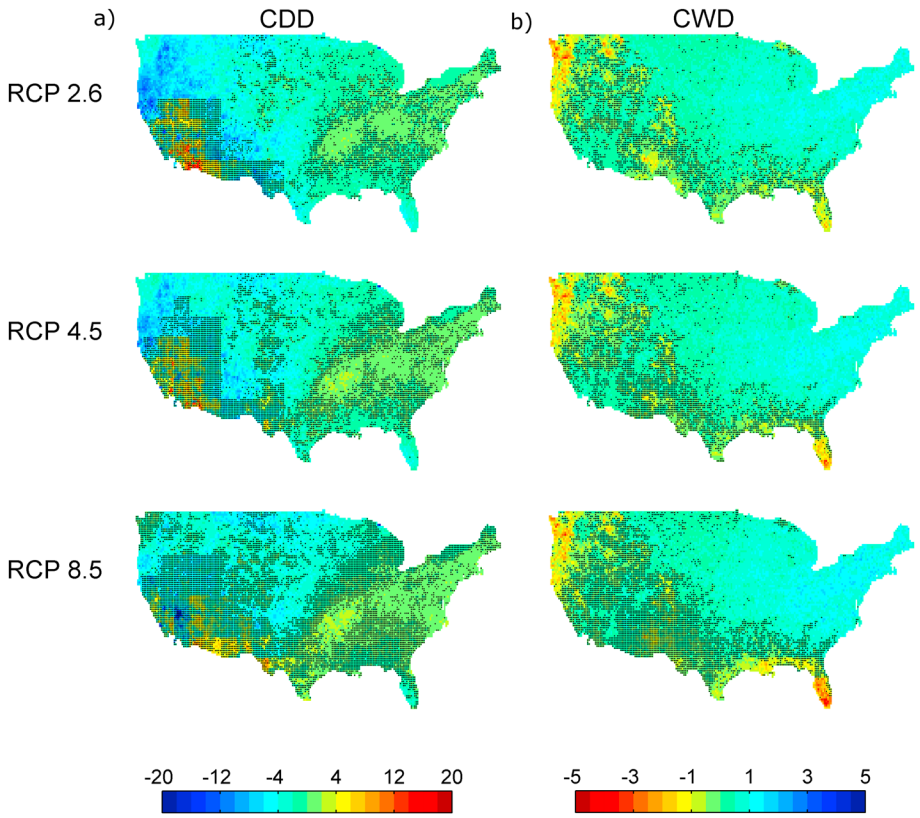

Figure 5. Projected changes in (a) the length of the average annual maximum dry spell length (CDD, in days) and (b) the length of the average annual maximum wet spell length (CWD, in days). Results are shown for the late 21st century (2066–2095) and for low, medium, and high levels of radiative forcing from greenhouse gases. Results are based on the ensemble mean of downscaled output from eight AOGCMs. Changes in hatched areas are not significant at the 95% level. Note that different scales are used in Figures 5a and 5b and that the scale in Figure 5b is reversed so that the blue colors always represent wetter conditions (i.e., shorter dry spells or longer wet spells).

spring, and the Southeast U.S. during autumn (c.f. Figures 6 and 4). Under the RCP 8.5 scenario, some of these regions are projected to have an additional six to ten 10 mm precipitation events with several additional 20 mm events. These findings are consistent with those of *Lau et al.* [2013] who report a global increase in heavy rainfall with increases on both the East and West Coasts of the U.S.

5. Summary and Discussion

High-resolution (0.25° × 0.25°) 21st century precipitation projections have been developed for the contiguous U.S. by scaling the descriptors of the precipitation occurrence and intensity processes and then stochastically generating daily precipitation time series. The downscaling approach was applied to output from eight CMIP5 models using three scenarios of 21st century greenhouse gas forcing. In terms of spatial pattern, the projections exhibit a strong level of agreement with their coarse-resolution counterparts but provide much greater detail for regional analysis. The downscaled series were also analyzed seasonally and in terms of changes in multiple metrics describing occurrence and intensity to provide insight into the projections.

The largest changes in annual precipitation totals are increases in the Northeast, Pacific Northwest, and in the high elevations of the Rocky Mountains. The magnitude of the increase is highly dependent on the level of radiative forcing from greenhouse gases. Parts of the Southern U.S. are projected to experience moderate precipitation decreases under all forcing scenarios. Increases in precipitation were further found to be associated primarily with changes in cold season precipitation, while significant precipitation decreases occurred in parts of the Southern U.S. in all seasons except autumn. Increases in precipitation were found to be associated primarily with the precipitation intensity process while decreases were found to be associated primarily with the precipitation occurrence process. Many locations in the Eastern U.S. are projected to

©2015. American Geophysical Union. All Rights Reserved.

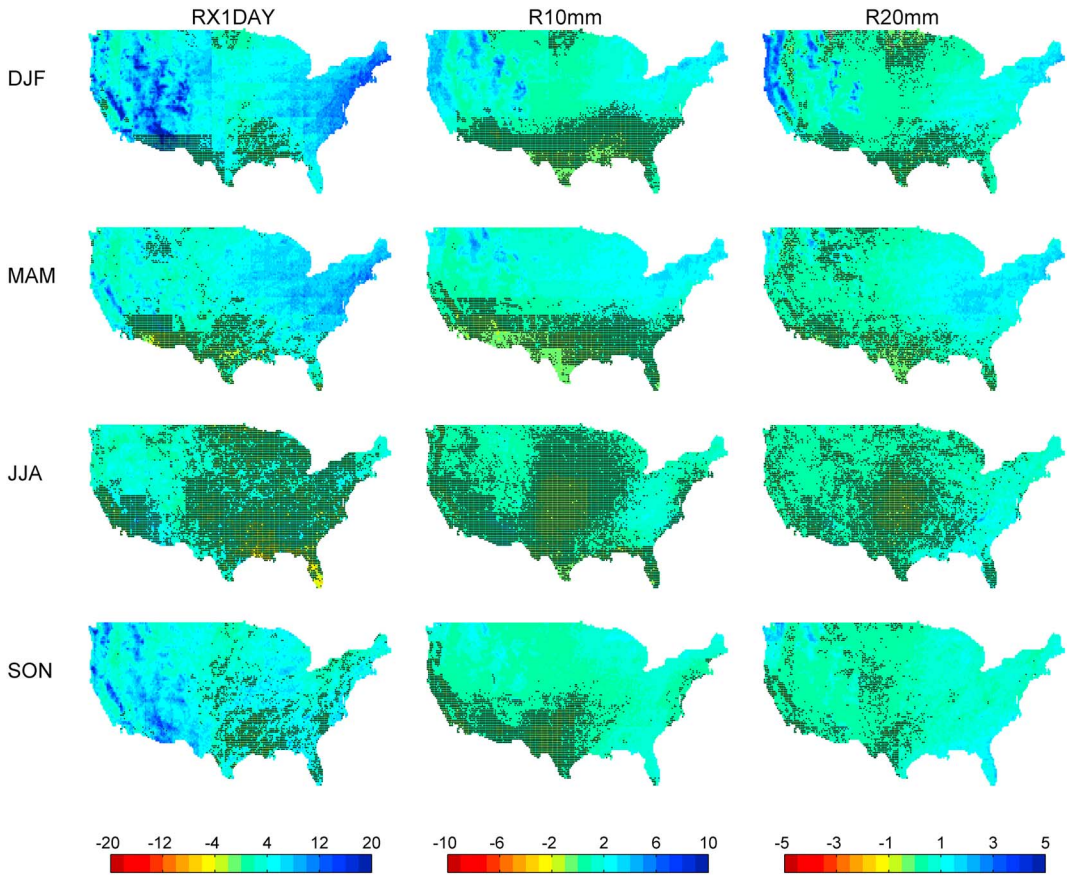

Figure 6. Projected changes in seasonal values of (left column) the average single largest precipitation event (RX1DAY; mm), (middle column) the number of heavy (>10 mm) precipitation events (R10mm), and (right column) the number of very heavy (>20 mm) precipitation events (R20mm) under high radiative forcing (RCP 8.5) for 2066–2095. Results are based on the ensemble mean of downscaled output from eight AOGCMs. Changes in hatched areas are not significant at the 95% level.

experience an increase in the length of extreme dry spells and an increase in the length of the longest wet spells, reflecting an increase in the serial correlation of precipitation. Many western locations, on the other hand, are projected to experience shorter dry spells and wet spells, reflecting a decrease in the serial correlation of precipitation. Most U.S. locations are projected to experience an increase in extreme precipitation, as manifest in changes in the mean annual single-day maximum precipitation, as well as the number of heavy (>10 mm) and very heavy (>20 mm) precipitation days.

In the canon of statistical downscaling techniques, the scaling approach applied here is relatively simple and practitioners should always be cognizant of the relative merits of different downscaling tools. The method applied in this paper focuses on improvement of (1) the spatial detail and (2) the representation of the daily precipitation process. Because the method is based on scaling of climate model output, areas characterized by sharp contrasts in the native climate model output will be similarly characterized in the high-resolution downscaled products. Impact studies, especially those focused on hydrology in large watersheds, often require spatially autocorrelated data. While the series described here are not related at neighboring grid points, several approaches exist and could be easily implemented to include spatial autocorrelation. The projections might also be used, in conjunction with projections of other variables, in crop modelling applications. The approach is also adaptable to even higher-resolution data, such as the new daily PRISM (Parameter-elevation Relationships on Independent Slopes Model) data with ~4 km resolution (see *Daly et al.* [2008] and prism.oregonstate.edu).

Given the computational expense of applying even a simple statistical downscaling approach to multiple models and radiative forcing trajectories, it is important to establish that value has been added. Several recent studies have presented smoothed or interpolated CMIP5 output for a range of precipitation metrics. The results of this study exhibit qualitative agreement with these analyses of raw CMIP5 data in terms of

©2015. American Geophysical Union. All Rights Reserved.

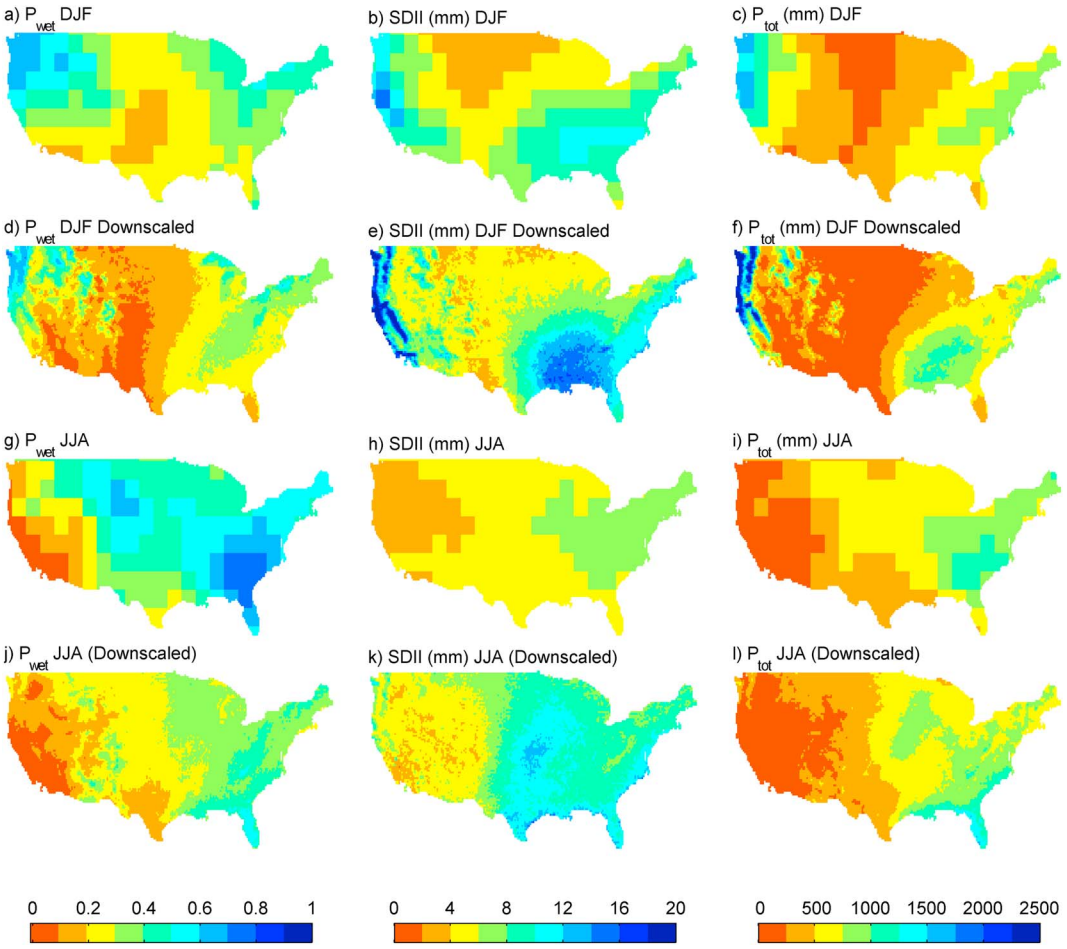

Figure 7. Projections of wet day probability (P_{wet}), the simple daily intensity index (SDII; mm), and the precipitation total (P_{tot}; mm) as derived from raw and downscaled CMIP5 models. The maps show the ensemble average from (a–c and g–i) eight CMIP5 models and (d–f and j–l) their downscaled counterparts. Results are shown for the winter (DJF) in the first two rows and for summer (JJA) in the last two rows.

regions where the models agree on the sign of change (cf. Figure 4 with Figure 2 of *Maloney et al.* [2014] and Figure 6 of this paper with Figure 7 of *Wuebbles et al.* [2014]). However, the approach presented here also adds spatial detail, especially in areas of topographic relief. Because the methodology also relates the precipitation statistics at coarse resolution to those at fine resolution, it improves the simulation of fine resolution wet day probability and mean wet day precipitation intensity relative to raw model output. As a demonstration of this added detail, Figure 7 shows the multimodel ensemble wet day probability (P_{wet}), mean wet day amount (SDII; mm), and the seasonal total (P_{tot}; mm) for winter (DJF) and summer (JJA). It is evident from Figure 7 that downscaling effectively improves the spatial detail present in the projections but also improves the models overestimation of precipitation occurrence and underestimation of intensity noted in the introduction.

In this paper, we have presented a relatively simple approach for deriving high-resolution precipitation projections and quantified the resulting changes in precipitation occurrence and intensity based on a multimember climate model ensemble. The physical processes associated with the projected changes are the subject of ongoing research. For example, *Li et al.* [2013] found that models differ substantially in their simulation of the North Atlantic subtropical high, resulting in differences in their simulation of precipitation variability in the Southeast U.S. Because precipitation depends not only on the presence of adequate atmospheric moisture but also on its transport to regions of convergence, it is likely that the results presented here are driven by a combination of changes in atmospheric moisture content and circulation changes. Additional work is needed to assess the relative contributions of these drivers to regional changes in

©2015. American Geophysical Union. All Rights Reserved.

precipitation and ultimately increase the confidence in such projections. Further work is also needed to compare the temporal and spatial characteristics of precipitation projections derived from the relatively simple downscaling approach presented here with projections derived using other methods that have been more widely applied for assessing hydrological impacts of changes in climate. Further work on the validity of the stationarity assumption underlying this and other statistical downscaling approaches is also now possible as a result of increasing GCM resolution and the development of "perfect model" approaches [e.g., *Barsugli et al.,* 2013] and should be the focus of additional future research. Lastly, the implications of the projections presented here will likely depend on changes in other variables, primarily air temperature. This is especially important for quantifying impacts at high elevations, where changes in temperature might impact the partitioning of frozen and liquid precipitation, with important consequences for regional hydrology. Development of high-resolution projections for temperature is the subject of ongoing research.

Acknowledgments

This material is based upon work supported by the National Science Foundation under grant 1009925. Any opinions, findings, and conclusions or recommendations expressed in this material are those of the author and do not necessarily reflect the views of the National Science Foundation. I acknowledge the World Climate Research Programme's Working Group on Coupled Modelling, which is responsible for CMIP, and thank the climate modeling groups (listed in section 2) for producing and making available their model output. For CMIP, the U.S. Department of Energy's Program for Climate Model Diagnosis and Intercomparison provided coordinating support and led the development of software infrastructure in partnership with the Global Organization for Earth System Science Portals. CPC U.S. Unified Precipitation data are provided by the NOAA/OAR/ESRL PSD, Boulder, Colorado, USA, from their Web site at http://www.esrl.noaa.gov/psd/. The author also acknowledges valuable feedback from three anonymous reviewers. In keeping with AGU's Data Policy, data used to produce the results of the paper are available from the author upon request.

References

Alexander, L. V., et al. (2006), Global observed changes in daily climate extremes of temperature and precipitation, *J. Geophys. Res.*, *111*, D05109, doi:10.1029/2005JD006290.

Arora, V. K., J. F. Scinocca, G. J. Boer, J. R. Christian, K. L. Denman, G. M. Flato, V. V. Kharin, W. G. Lee, and W. F. Merryfield (2011), Carbon emission limits required to satisfy future representative concentration pathways of greenhouse gases, *Geophys. Res. Lett.*, *38*, L05805, doi:10.1029/2010GL046270.

Barsugli, J. J., et al. (2013), The practitioner's dilemma: How to assess the credibility of downscaled climate projections, *Eos Trans. AGU*, *94*, 424–425, doi:10.1002/2013EO460005.

Bentsen, M., et al. (2013), The Norwegian Earth System Model, NorESM1-M – Part I: Description and basic evaluation of the physical climate, *Geosci. Model Dev.*, *6*, 687–720, doi:10.5194/gmd-6-687-2013.

Cayan, D. R., T. Das, D. W. Pierce, T. P. Barnett, M. Tyree, and A. Gershunov (2010), Future dryness in the southwest US and the hydrology of the early 21st century drought, *Proc. Natl. Acad. Sci. U.S.A.*, *107*, 21,271–21,276, doi:10.1073/pnas.0912391107.

Collins, M., et al. (2013), Long-term climate change: Projections, commitments and irreversibility, in *Climate Change 2013: The Physical Science Basis. Contribution of Working Group I to the Fifth Assessment Report of the Intergovernmental Panel on Climate Change*, edited by T. F. Stocker et al., pp. 1029–1136, Cambridge Univ. Press, Cambridge, U. K., and New York.

Cressman, G. F. (1959), An operational objective analysis system, *Mon. Weather Rev.*, *87*, 367–374.

Daly, C., M. Halbleib, J. I. Smith, W. P. Gibson, M. K. Doggett, G. H. Taylor, J. Curtis, and P. P. Pasteris (2008), Physiographically sensitive mapping of climatological temperature and precipitation across the conterminous United States, *Int. J. Climatol.*, doi:10.1002/joc.1688.

Dufresne, J.-L., et al. (2012), Climate change projections using the IPSL-CM5 Earth System Model: From CMIP3 to CMIP5, *Clim. Dyn.*, *40*, 2123–2165, doi:10.1007/s00382-012-1636-1.

Easterling, D. R., G. A. Meehl, C. Parmesan, S. A. Changnon, T. R. Karl, and L. O. Mearns (2000), Climate extremes: Observations, modeling, and impacts, *Science*, *289*, 2068, doi:10.1126/science.289.5487.2068.

Frich, P., L. V. Alexander, P. Della-Marta, B. Gleason, M. Haylock, A. M. G. Klein Tank, and T. Peterson (2002), Observed coherent changes in climatic extremes during the second half of the twentieth century, *Clim. Res.*, *19*, 193–212.

Gabriel, K. R., and J. Neumann (1962), A Markov chain model for daily rainfall occurrence at Tel Aviv, *Q. J. R. Meteorol. Soc.*, *88*, 90–95.

Groisman, P. Y., R. W. Knight, and T. R. Karl (2012), Changes in intense precipitation over the Central United States, *J. Hydrometeorol.*, *13*, 47–66, doi:10.1175/JHM-D-11-039.1.

Gutmann, E. G., T. Pruitt, M. P. Clark, L. Brekke, J. R. Arnold, D. A. Raff, and R. M. Rasmussen (2014), An intercomparison of statistical downscaling methods used for water resource assessments in the United States, *Water Resour. Res.*, *50*, 7167–7186, doi:10.1002/2014WR015559.

Harding, K. J., P. K. Snyder, and S. Liess (2013), Use of dynamical downscaling to improve the simulation of U.S. warm season precipitation in CMIP5 models, *J. Geophys. Res. Atmos.*, *118*, 12,522–12,536, doi:10.1002/2013JD019994.

Hartmann, D. L., et al. (2013), Observations: Atmosphere and surface, in *Climate Change 2013: The Physical Science Basis. Contribution of Working Group I to the Fifth Assessment Report of the Intergovernmental Panel on Climate Change*, edited by T. F. Stocker et al., Cambridge Univ. Press, Cambridge, U. K., and New York.

Hidalgo, H. G., M. D. Dettinger, and D. R. Cayan (2008), Downscaling with constructed analogues: Daily precipitation and temperature fields over the United States, *Report CEC-500-2007-123*, 48 pp., California Energy Commission, Sacramento, Calif.

Higgins, R. W., W. Shi, E. Yarosh, and R. Joyce (2000), *Improved US Precipitation Quality Control System and Analysis*, NCEP/Clim. Predict. Cent. ATLAS No. 7, National Centers for Environmental Prediction, Climate Prediction Center, Camp Springs, Md. [Available at http://www.cpc.noaa.gov/research_papers/ncep_cpc_atlas/7/index.html.]

Klein Tank, A. M. G., F. W. Zwiers, and X. Zhang (2009), Guidelines on analysis of extremes in a changing climate in support of informed decisions for adaptation, Climate data and monitoring WCDMP-No. 72, WMO-TD No. 1500, 56 pp.

Knutti, R., D. Masson, and A. Gettelman (2013), Climate model genealogy: Generation CMIP5 and how we got there, *Geophys. Res. Lett.*, *40*, 1194–1199, doi:10.1002/grl.50256.

Kunkel, K. E., et al. (2013), Monitoring and understanding trends in extreme storms, *Bull. Am. Meteorol. Soc.*, *94*, 499–514, doi:10.1175/BAMS-D-11-00262.1.

Lau, W. K.-M., H.-T. Wu, and K.-M. Kim (2013), A canonical response of precipitation characteristics to global warming from CMIP5 models, *Geophys. Res. Lett.*, *40*, 3163–3169, doi:10.1002/grl.50420.

Li, L., W. Li, and Y. Deng (2013), Summer rainfall variability over the Southeastern United States and its intensification in the 21st century as assessed by CMIP5 models, *J. Geophys. Res. Atmos.*, *118*, 340–354, doi:10.1002/jgrd.50136.

Maloney, E. D., et al. (2014), North American climate in CMIP5 experiments: Part III: Assessment of twenty-first century projections, *J. Clim.*, *27*, 2230–2270.

Maraun, D., et al. (2010), Precipitation downscaling under climate change: Recent developments to bridge the gap between dynamical models and the end user, *Rev. Geophys.*, *48*, RG3003, doi:10.1029/2009RG000314.

Maurer, E. P., and H. G. Hidalgo (2008), Utility of daily vs. monthly large-scale climate data: An intercomparison of two statistical downscaling methods, *Hydrol. Earth Syst. Sci.*, *12*, 551–563.

©2015. American Geophysical Union. All Rights Reserved.

Meehl, G. A., J. M. Arblaster, and C. Tebaldi (2005), Understanding future patterns of increased precipitation intensity in climate model simulations, *Geophys. Res. Lett.*, *32*, L18719, doi:10.1029/2005GL023680.
Mehran, A., A. AghaKouchak, and T. J. Phillips (2014), Evaluation of CMIP5 continental precipitation simulations relative to satellite-based gauge-adjusted observations, *J. Geophys. Res. Atmos.*, *119*, 1695–1707, doi:10.1002/2013JD021152.
Moss, R. H., et al. (2010), The next generation of scenarios for climate change research and assessment, *Nature*, *463*, 747–756.
Osborn, T. J., and M. Hulme (1997), Development of a relationship between station and grid-box rainday frequencies for climate model evaluation, *J. Clim.*, *10*, 1885–1908.
Parmesan, C., T. L. Root, and M. R. Willig (2000), Impacts of extreme weather and climate on terrestrial biota, *Bull. Am. Meteorol. Soc.*, *81*, 443–450.
Polade, J. D., D. W. Pierce, D. R. Cayan, A. Gershunov, and M. D. Dettinger (2014), The key role of dry days in changing regional climate and precipitation regimes, *Sci. Rep.*, *4*, 4364, doi:10.1038/srep04364.
Pryor, S. C., R. J. Barthelmie, and J. T. Schoof (2013), High-resolution projections of climate-related risks for the Midwestern USA, *Clim. Res.*, *56*, 61–79.
Schoof, J. T. (2013), Statistical downscaling in climatology, *Geogr. Compass*, *7*, 249–265, doi:10.1111/gec3.12036.
Schoof, J. T., and S. C. Pryor (2008), On the proper order of Markov chain model for daily precipitation occurrence in the contiguous United States, *J. Appl. Meteorol. Climatol.*, *47*, 2477–2486, doi:10.1175/2008JAMC1840.1.
Scoccimarro, E., S. Gualdi, A. Bellucci, M. Zampieri, and A. Navarra (2013), Heavy precipitation events in a warmer climate: Results from CMIP5 models, *J. Clim.*, *26*, 7902–7911, doi:10.1175/JCLI-D-12-00850.1.
Sillmann, J., V. V. Kharin, X. Zhang, F. W. Zwiers, and D. Bronaugh (2013a), Climate extremes indices in the CMIP5 multimodel ensemble: Part 1. Model evaluation in the present climate, *J. Geophys. Res. Atmos.*, *118*, 1716–1733, doi:10.1002/jgrd.50203.
Sillmann, J., V. V. Kharin, F. W. Zwiers, X. Zhang, and D. Bronaugh (2013b), Climate extremes indices in the CMIP5 multimodel ensemble: Part 2. Future climate projections, *J. Geophys. Res. Atmos.*, *118*, 2473–2493, doi:10.1002/jgrd.50188.
Stephens, G. L., T. L. L'Ecuyer, R. Forbes, A. Gettlemen, J.-C. Golaz, A. Bodas-Salcedo, K. Suzuki, P. Gabriel, and J. Haynes (2010), Dreary state of precipitation in global models, *J. Geophys. Res.*, *115*, D24211, doi:10.1029/2010JD014532.
Stevens, B., et al. (2013), The atmospheric component of the MPI-M Earth System Model: ECHAM6, *J. Adv. Model. Earth Syst.*, *5*, 146–172, doi:10.1002/jame.20015.
Stoner, A. M. K., K. Hayhoe, X. Yang, and D. J. Wuebbles (2013), An asynchronous regional regression model for statistical downscaling of daily climate variables, *Int. J. Climatol.*, *33*, 2473–2494, doi:10.1002/joc.3603.
Taylor, K. E., R. J. Stouffer, and G. A. Meehl (2012), An overview of CMIP5 and the experimental design, *Bull. Am. Meteorol. Soc.*, *93*, 485–498.
Tebaldi, C., and C. M. Arblaster (2014), Pattern scaling: Its strengths and limitations, and an update on the latest model simulations, *Clim. Change*, *122*, 459–471.
Tebaldi, C., K. Hayhoe, J. M. Arblaster, and G. A. Meehl (2006), Going to the extremes. An intercomparison of model simulated historical and future changes in extreme events, *Clim. Change*, *79*, 185–211, doi:10.1007/s10584-006-9051-4.
Thrasher, B., E. P. Maurer, C. McKellar, and P. Duffy (2012), Technical note: Bias correcting climate model simulated daily temperature extremes with quantile mapping, *Hydrol. Earth Syst. Sci.*, *16*, 3309–3314, doi:10.5194/hess-16-3309-2012.
Toreti, A., P. Naveau, M. Zampieri, A. Schindler, E. Scoccimarro, E. Xoplaki, H. A. Dijkstra, S. Gualdi, and J. Luterbacher (2013), Projections of global changes in precipitation extremes from Coupled Model Intercomparison Project Phase 5 models, *Geophys. Res. Lett.*, *40*, 4887–4892, doi:10.1002/grl.50940.
Villarini, G., J. A. Smith, and G. A. Vecchi (2013), Changing frequency of heavy rainfall over the Central United States, *J. Clim.*, *26*, 351–357, doi:10.1175/JCLI-D-12-00043.1.
Voldoire, A., et al. (2012), The CNRM-CM5.1 global climate model: Description and basic evaluation, *Clim. Dyn.*, *40*, 2091–2121.
von Salzen, K., et al. (2013), The Canadian fourth generation Atmospheric Global Climate Model (CanAM4). Part I: Representation of physical processes, *Atmos. Ocean*, *51*, 104–125.
Warrick, R. A., W. Ye, P. Kouwenhoven, J. E. Hay, and C. Cheatham (2005), New developments of the SimCLIM model for simulating adaptation to risks arising from climate variability and change, in *MODSIM 2005. International Congress on Modelling and Simulation*, edited by A. Zerger and R. M. Argent, pp. 170–176, Modelling and Simulation Society of Australia and New Zealand. [Available at www.mssanz.org.au/modsim05/.]
Wilks, D. S. (1999a), Interannual variability and extreme-value characteristics of several stochastic daily precipitation models, *Agric. For. Meteorol.*, *93*, 153–169.
Wilks, D. S. (1999b), Multisite downscaling of daily precipitation with a stochastic weather generator, *Clim. Res.*, *11*, 125–136.
Wilks, D. S. (2010), Use of stochastic weather generators for precipitation downscaling, *WIREs Clim. Change*, *1*, 898–907, doi:10.1002/wcc.85.
Wuebbles, D., et al. (2014), CMIP5 climate model analyses: Climate extremes in the United States, *Bull. Am. Meteorol. Soc.*, *95*, 571–583.
Xin, X., T. Wu, J. Li, Z. Wang, W. Li, and F. Wu (2012), How well does BCC_CSM1.1 reproduce the 20th century climate change over China?, *Atmos. Oceanic Sci. Lett.*, *6*, 21–26.
Yukimoto, S., et al. (2012), A new global climate model of the Meteorological Research Institute: MRI-CGCM3 - Model description and basic performance, *J. Meteorol. Soc. Jpn.*, *90A*, 23–64.

©2015. American Geophysical Union. All Rights Reserved.